ARTICLES

Equation of state of ice VII up to 106 GPa

E. Wolanin, Ph. Pruzan, J. C. Chervin, B. Canny, and M. Gauthier
Physique des Milieux Condensés, Université Pierre et Marie Curie, B 77, 4 place Jussieu, 75252 Paris, Cedex 05, France

D. Häusermann and M. Hanfland
ESRF, BP 220, 38043 Grenoble Cedex, France
(Received 9 January 1997)

Using angle-dispersive x-ray powder diffraction and image plate detector, the equations of state of H_2O and D_2O ice VII, corrected for deviatoric strain, were determined up to 106 GPa, and 60 GPa, respectively. Our data were analyzed on the basis of the universal equation of state of Vinet *et al.* This treatment indicates the occurrence of two second- or higher-order phase transitions at about 15 and 66 GPa, in agreement with the pressure ranges where the nature of the proton disorder is expected to change. [S0163-1829(97)08034-X]

INTRODUCTION

Although at low pressure the phase diagram of ice exhibits a rich polymorphism,[1] above 2.1 GPa it simplifies down to only two solids: cubic ice VII (space group $Pn\overline{3}m$) with two molecules per unit cell on site symmetry $\overline{4}3m$,[2,3] and, below 270 K, tetragonal ice VIII (space group $I4_1/amd$) with eight molecules per unit cell on site symmetry mm.[2] Ice VII is a proton-disordered paraelectric solid, whereas ice VIII is an antiferroelectric proton-ordered phase. The VII-VIII transition line was recently determined by Raman scattering.[4] The T_c vs p curve shows marked slope changes at about 15 and 60 GPa (20 and 70 GPa for D_2O), suggesting three regimes for the order-disorder transformation, which may be correlated to the nature of the proton disorder in ice VII. Around 2.4 GPa, as shown by neutron diffraction analysis,[2] ice VII is orientationally disordered. Due to the increase of the intermolecular forces with pressure, the rotational tunneling is expected to decrease as observed for instance in methane.[5] Actually, a change of slope of T_c vs p is found around 15 GPa, and on further compression the variation of T_c is similar to what is found in H-bonded ferroelectric compounds such as KH_2PO_4 :[6,7] first, T_c decreases linearly with p, then at a critical pressure, which is about 62 GPa for H_2O, it drops to 0 K. As shown by the Ising model with a double-well proton potential, the linear regime is accounted for by the mere compression of the intermolecular distance $d_{\text{O-O}}$ with constant covalent-bond length.[8] From the following observations this regime would correspond to a quasistatic disorder: (i) as a rule, the orientational disorder observed at low pressure is expected to decrease as pressure increases; (ii) the linear regime is described by a Hamiltonian containing only a dipolar interaction (Ising term); in other words there is no need for a dynamical disorder term to determine the transition temperature T_c. At T_c, the long-range dipolar order of ice VIII disappears and, due to the ice rule, is replaced by a short-range order in ice VII. The tunneling energy, small compared to the dipolar interaction, may, however, play a role in the reordering of the short-range order domains. Around 62 GPa (72 GPa for D_2O), the impossibility to order the system, even at zero temperature, may be ascribed to the proximity of the proton double-well barrier's height to the proton zero-point energy. This causes the delocalization of the proton along the bond, preventing the stabilization of the ordered phase. From earlier theoretical computation by Schweizer and Stillinger,[9] this pressure was estimated around 33 GPa; extrapolation of a recent *ab initio* computation by Silvi and Besson *et al.*[10,11] allows a better estimation at around 70 GPa. On further compression, it is expected that this solid should lead to the symmetric ordered phase, the so-called ice X, referred to in the following as ordered ice X (Cu_2O structure), in which the proton lies at the midpoint between two oxygens. Schweizer and Stillinger found that the symmetric solid is obtained at 45 GPa, where the proton density was found peaked at the bond center.[9] Vibrational spectroscopies are relevant methods to characterize the behavior of ice at ultrahigh pressure. Presently, no significant peak of ice X was found with Raman spectroscopy up to 130 GPa;[12] on the other hand, Aoki *et al.*[13] and Goncharov *et al.*[14] concluded from infrared spectroscopy that ice X is reached around 60–62 GPa. This point is discussed later on in connection with the proton ordering.

The expected phase transitions mentioned above and occurring at 15 and 60 GPa for H_2O, which are very likely second- or higher-order transformations, may have detectable effects on the equation of state (EOS). In order to investigate the possible existence of such effects, we have determined the EOS of ice VII up to 106 GPa using angular dispersive powder diffraction (ADX) and high brilliance synchrotron radiation. The equation of state of ice was already determined by Liu,[15] Munro *et al.*,[16] and up to 128 GPa by Hemley *et al.*[17] In the latter work, only the 110 diffraction peak was observed using energy dispersive x-ray diffraction (EDX) and synchrotron radiation. Data of Hemley *et al.* were reanalyzed by Hama and Suito;[18] this work is discussed

in the last section. In the present work a more powerful technique than EDX was used: ADX combined with image plate detectors allows the observation of a larger number of reflections with more reliable intensities, hence leading to more accurate crystallographic and volume data. Several sets of data were collected at the European Synchrotron Radiation Facility (ESRF, Grenoble, France) on H_2O and D_2O, up to 106 GPa and 60 GPa, respectively. The 110, 200, and 211 reflections were followed up to the highest pressures, allowing us to perform deviatoric strain correction. Treatment of the final data based on the EOS of Vinet[19] supports our scheme on the evolution of the proton disorder nature, drawn from the pressure dependence of the VII-VIII transition temperature T_c.

EXPERIMENT

The high-pressure devices used in these experiments were diamond anvil cells (DAC) with two wide conical apertures on the symmetry axis of the system. Two different cell designs were used: (i) a membrane type DAC (MDAC) designed in our laboratory,[20] with tungsten carbide seats and a full (4θ) x-ray aperture of 56°; (ii) a Diacell (DXR-5), with beryllium seats, and maximum aperture of 90°. A preindented stainless-steel gasket confined the sample [tridistilled H_2O or 99.80% isotopic purity D_2O from Euriso-top (CEA, France)] into a 50-μm-diam hole. A small (~ 5 μm) ruby chip was placed into the hole for *in situ* pressure measurement according to the shift of the ruby luminescence R_1 line, using the five-power law.[21]

Synchrotron radiation, with its high intensity and low beam divergence, is required for this low-Z material. High pressure powder diffraction was performed in an angle-dispersive mode at the ESRF on beam line ID9, using a large area (340×400 mm^2) image plate. The monochromatic x-ray beam ($\lambda\sim 0.4$ Å), parallel to the symmetry axis of the DAC, was collimated down to 50×50 μm^2 and cleaned up close to the cell using fine slits to avoid gasket signal. During exposure times, the cell was rocked through $\pm$ 3° in order to improve the crystallite averaging, the limited range of 3° being chosen to avoid diamond reflections. At room temperature, four runs were performed with H_2O, up to a maximum pressure of 106 GPa, and two runs with D_2O, up to 60 GPa. A silicon powder standard was used to determine the wavelength and sample-to-plate distance.

RESULTS AND DATA TREATMENT

Data were collected on image plates in about 1 h. The two-dimensional powder rings were integrated into a conventional profile (shown at 7 GPa in inset in Fig. 1) through programs PLATYPUS[22] or FIT2D.[23] Indexation of the peaks was consistent with the primitive cubic lattice. The recorded intensities were observed to be uniform around the powder rings, indicating that the quality of the powder was good. However, a slight preferred orientation effect along the [100] direction was found, as indicated by the comparison of the relative intensities of the peaks with a simulation performed using program FULLPROF.[24] The x-ray aperture of our membrane DAC permitted us to follow the 110, 200, and 211 diffraction lines of the ice VII cubic lattice up to 106 GPa. At

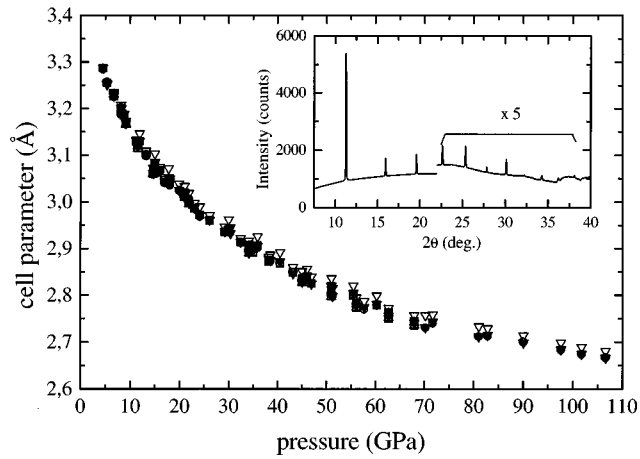

FIG. 1. Cell parameter computed from various hkl diffraction lines; hollow circle: 110; filled circle: 111; hollow down triangle: 200; filled down triangle: 211; hollow square: 220; filled square: 310; hollow up triangle: 222; filled up triangle: 321; inset: H_2O spectrum at 6.7 GPa with the Diacell DAC.

lower pressures, a greater number of reflections were observed. Below 10 GPa, 14 diffraction lines were collected using the Diacell (see inset in Fig. 1), while five peaks were observed with the MDAC up to 60 GPa. The 111 diffraction line, assigned to the hydrogen atoms, was followed up to 18 GPa, where it became too faint to be observed. Moreover, on some runs we could observe a slight splitting of the 110 peak into a doublet, likely to be attributed to the combined effect of preferred orientation and deviatoric stress; such a combination would also stand for the larger value of the cell parameter computed from the 200 diffraction line, which cannot be accounted for by only using Eq. (2) (see below).

The cell parameter of the cubic lattice was computed from each hkl (Muller indices) diffraction line. Error on the cell parameter, estimated only from the precision on the hkl diffraction line position, depends on the pressure range: at 20, 80, and 100 GPa, it is ±0.002, ±0.005, and ±0.01 Å, respectively. However, systematic differences between the computed cell parameters were observed (see Fig. 1). These systematic differences are ascribed to the presence of a uniaxial stress component (USC) t along the loading direction, caused by the compression system.[25,26] This USC has to be taken into account to obtain the corrected value of the cell parameter under the hydrostatic pressure p_{hydr} given by

$$p_{hydr}=p_{meas}-\tfrac{1}{3}t, \tag{1}$$

where p_{meas} is the measured pressure determined from the ruby line. The USC was calculated from our diffraction data using Eqs. (2), (3), and (4) given below, which were derived by Singh and Balasingh for cubic systems.[27] In our geometry, termed parallel geometry, the load direction coinciding with the direction of the incident x-ray beam, the cell parameter computed from a hkl reflection is given by

$$a_{hkl}=a_{hydr}+ta_0[s_{11}+(s_{12}-s_{11})\cos^2\theta_B + S(1-3\sin^2\theta_B)\Gamma], \tag{2}$$

with

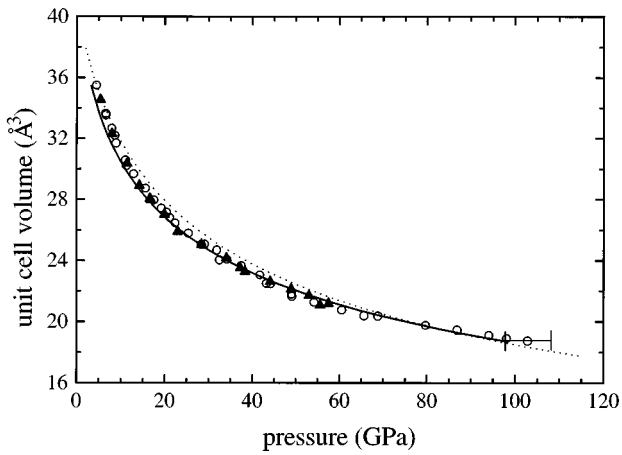

FIG. 2. Corrected unit cell volume vs corrected (hydrostatic) pressure; circles: H_2O; triangles: D_2O; solid line: least square fit to a Birch-Murnaghan EOS (B_0=14.9 GPa taken from Shimizu *et al.*; fitted parameters: B_0'=5.4 and a_0=3.45 Å); dashed line: Hemley *et al.* data. For clarity reasons, error bar on the pressure is indicated only on the last data point; the error on the pressure depends on the range: at 10, 40, 100 GPa, it is ±0.5, ±2 and ±10 GPa, respectively; the error on the volume is inferior, or equal at high pressure, to the symbol diameter.

$$S = s_{11} - s_{12} - \tfrac{1}{2} s_{44}, \tag{3}$$

$$\Gamma = \frac{h^2k^2 + h^2l^2 + k^2l^2}{(h^2+k^2+l^2)^2}, \tag{4}$$

where a_{hkl} represents the experimental cell parameter for the hkl reflection, a_{hydr} the cell parameter under hydrostatic conditions, a_0 is the cell parameter at zero pressure which was taken as 3.44 Å from Hemley *et al.*;[17] s_{ij} are the elastic compliances, and θ_B the corresponding Bragg angle. To compute t, the pressure dependence of the compliances or of the elastic coefficients has to be known. The recent results of Shimizu and co-workers[28,29] performed up to 7 GPa for both H_2O and D_2O were used, and a linear pressure dependence of the elastic coefficients up to 106 GPa was assumed. The incompressibility coefficient B being a linear combination of the elastic coefficients for a cubic material ($B=(c_{11}+2c_{12})/3$), this latter assumption involved a linear pressure dependence of B which is usually assumed. The error on the deviatoric strain correction on a_0 is discussed in the following section.

Using the various diffraction lines, Eq. (2) was fitted at each pressure with t and a_{hydr} as parameters. Thus the USC and the hydrostatic cell parameter were obtained as functions of pressure. Within the scatter of the computed points, the USC was found to have a linear pressure dependence: in the whole pressure range, t was found around 10% of the measured pressure. The computed cell volume $(a_{hydr})^3$ as a function of the hydrostatic pressure is plotted in Fig. 2. The difference between the corrected and uncorrected volume is about 1%. Figure 2 shows a very good agreement between the various runs; no isotope-related difference was observed within the present experimental accuracy.

TABLE I. Values of the parameters a_0 and B_0' in Eqs. (A1) and (A2) derived from the fit of our data for ice VII H_2O and D_2O (B_0 taken from Shimizu *et al.*[28]).

	Birch-Murnaghan	Vinet
B_0 (GPa)	14.9±0.8	14.9±0.8
B_0'	5.4±0.1	6.2±0.1
a_0 (Å)	3.451±0.008	3.427±0.008
Mean relative error (GPa)	1.60	1.86
Maximum relative error (GPa)	5.22	5.91

DISCUSSION

The corrected volume vs hydrostatic pressure was first fitted to a Birch-Murnaghan EOS (see Appendix), using for the isothermal bulk modulus at zero pressure the value B_0 of 14.9 GPa derived from the elastic coefficients of Shimizu *et al.* [28] The fitted parameters were B_0', the first pressure derivative of the bulk modulus, and a_0, the cell parameter at zero pressure; the results of the fit are given in Table I. We note that the value B_0 of 14.9 GPa is well below the 23.7 GPa value proposed by Hemley *et al.* from their x-ray data. If this latter value of 23.7 GPa is used, the fit of our data provides $B_0'=4.8\pm0.1$, and $a_0=3.373\pm0.008$ Å, with a mean relative error of 1.81 GPa and a maximum relative error of 5.5 GPa. However, the large difference between 23.7 and 14.9 has only a weak influence on our calculations; e.g., if we impose the value of 23.7 GPa for B_0, the computed uniaxial stress differs by ~ 5% and the corrected cell parameter variation is less than 0.02%. Moreover, the value of 14.9 GPa is well within the range of bulk moduli obtained for other phases of ice.[30,31] Compared to the Hemley *et al.* data, our results show a more compressible behavior in the 10–40 GPa range, and a stiffer one above 80 GPa. However, their data were uncorrected for deviatoric strain; if a 3% [see Eq. (1)] correction on the pressure is applied to the Hemley data, the difference between their (corrected) EOS and ours is less marked. In Table I, B_0' and a_0 are also given when using a Vinet EOS (see Appendix). The pressure dependence of our volume data appears to be regular and apparently does not show any sign suggesting phase transitions in the expected ranges. To proceed further, we followed the treatment derived by Vinet *et al.*,[32] and used by Hama and Suito[18] for ice VII. This treatment is based on the fact that in the system of coordinates $\ln(H(x))$ vs $(1-x)$, where $x=a/a_0$ and

$$H(x) = \frac{px^2}{3(1-x)}, \tag{5}$$

the Vinet EOS, in the absence of phase transition, must be linear. The plot of our data in this system of coordinates is presented in Fig. 3 for H_2O. Three linear regimes are clearly observed. Slope changes occur around $1-x=0.095$ and $1-x=0.20$, i.e., 12 GPa and 66 GPa, respectively. D_2O data are being processed, and first results would indicate a shift in pressure of about 5 GPa in the lower region and of about 15 GPa in the upper region. This behavior, together with the smooth variation observed in Fig. 2 as well as in Fig. 3 where the turns are not very sharp, supports the existence of second- or higher-order phase transitions, as inferred by the

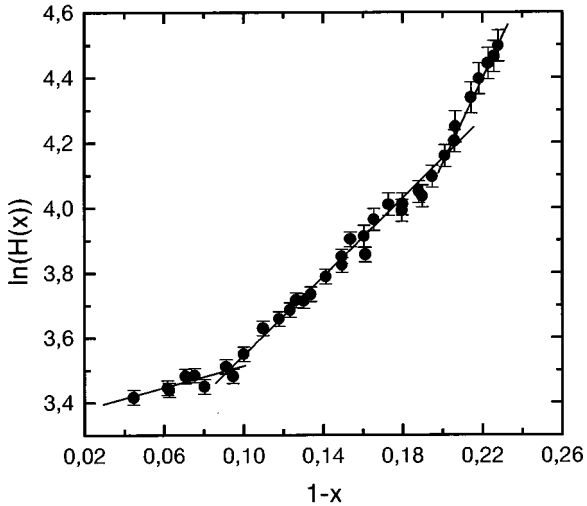

FIG. 3. Plot $\ln(H(x))$ vs $(1-x)$ [see Eqs. (5) and (A2)] for ice VII H_2O at room temperature; line: manual fit.

analysis of the pressure dependence of the VII-VIII transition temperature. The pressure range being separated into three zones, we fit each one with a Vinet EOS, with the starting point taken at the transition pressure p_t. The Vinet EOS [see Eq. (A2)] is then expressed as

$$p-p_t=\frac{3B_0(1-x)}{x^2}\exp[\tfrac{3}{2}(B_0'-1)(1-x)], \qquad (6)$$

where $x=a/a_t$, and a_t is the lattice parameter at p_t. Results of these fits are given in Table II. Due to the few number of points left in each zone, error margins on B_0' are relatively large. The parameters B_0 and B_0' increase significantly with pressure; specifically it is worth recalling that B_0', which is representative of the nature of the interatomic potential,[33] is expected to increase at high pressure. Hama and Suito, applying the same type of treatment to the data of Hemley *et al.*, concluded that phase changes occurred at 40 and 70 GPa. Performing the same treatment on the Hemley data, we found a slope change around 70 GPa; on the other hand, the lower pressure feature is not clearly apparent. We must stress also that the conclusions of Hama and Suito, concerning the suggested phase transition sequence ice VII → symmetric ice → proton disordered symmetric ice, are very likely not correct. Assuming a symmetrical double-well potential for the proton, the potential barrier decreases with increasing pressure, thus favoring first the delocalization of the proton along the O-O axis, as shown by the sudden decrease of $T_c(p)$ in the phase diagram. On further compression, as recalled in the Introduction, the proton density is expected to have only one maximum at the center of the O-O distance, and this latter transformation should lead to a symmetric ordered phase of cuprite structure. The zone found above 66 GPa (Fig. 3) is very likely the disordered form of the symmetric phase, with the delocalized proton statistically centered between two oxygens. At this point it is useful to recall the dynamical properties of the expected ordered ice X compared to what is observed with Raman and infrared spectroscopies above 60 GPa. In ice X [Cu_2O structure, $\overline{4}3m(T_d)$ oxygen site symmetry and $\overline{3}m(D_{3d})$ hydrogen site symmetry], one triply degenerate Raman active mode F_{2g} and two triply degenerate infrared active modes F_{1u} are expected.[34] The Raman mode is due solely to the oxygen sublattice vibration, whereas the infrared modes are due to both hydrogen and oxygen sublattices vibrations (translational and distortional).[13] Starting from ordered ice VIII, the F_{2g} mode originates from the translational lattice vibrations and the F_{1u} modes from the stretching vibrations (for the translational motion) and from the bending and librational vibrations (for the distortional motion). The experimental observations are the following:

(1) On increasing pressure on ice VII from 20 GPa, the lattice and stretching Raman active mode intensities were found to progressively decrease with a broadening of the stretching mode.[3,8,12] A strong broadening of the infrared stretching peak is also observed.[13] Above 50 GPa up to 130 GPa, the upper limit of our investigation, no significant Raman peak was found,[8,12] in particular the F_{2g} mode was not observed.

(2) Raman investigation of the phase diagram has shown that ice VIII, the ordered form of ice VII, vanished above a critical pressure close to 62 GPa (72 GPa for D_2O).[4,12]

(3) According to the infrared investigations the distortional F_{1u} mode was observed from 60 GPa, the vibrational mode from 90 GPa.[13] However, locations of the occurrence of these modes are not accurate because investigations were performed from 700 cm^{-1} and the respective ν vs p curves lie on the extrapolations of the translational and librational modes of ice VII (or VIII).

(4) The F_{1u} modes are very broad; narrowing and increase in intensity of the distortional mode occur from 65 GPa; the same behavior is observed for the translational mode above 90 GPa.[13]

The infrared measurements[13,14] demonstrate that a transformation around 60 GPa (70 GPa for D_2O) occurs. The intensity variations of the F_{1u} modes (point 4) are relevant observations for the location and the characteristics of this transformation. The broadening of the Raman and the infrared stretching peaks on approaching the transition from below and the absence of Raman peaks around 60 GPa (point 1) indicate the evolution to a disordered solid; the evolution of the infrared peaks above this pressure domain confirms that feature and suggests a progressive ordering on further compression (point 4). The transformation to a disordered solid at ~60 GPa is consistent with the limit of stability found for ice VIII, suggesting a delocalization of the proton site (point 2).[4,8,12] The statement given by Aoki *et al.* that ordered ice X is reached at 60 GPa relies on the change of sign of the stretching frequency pressure dependence; actually the translational mode is observed around 90 GPa, not

TABLE II. Values of the parameters B_0 and B_0' in Eq. (A2) derived from the fit of our data for ice VII in each zone of Fig. (3).

	0–13 GPa	13–66 GPa	>66 GPa
B_0 (GPa)	27.8±1.4	97±4	260±20
B_0'	2.8±0.4	3.0±0.3	7.3±1.8
Mean relative error (GPa)	0.3	1.0	0.6
Maximum relative error (GPa)	0.9	2.1	1.2

around 60 GPa. In contrast to Aoki *et al.*, Goncharov *et al.*,[14] from the behavior of the translational and distortional modes beyond 100 GPa, concluded that the ordered solid (static symmetric bonds) may occur around 150 GPa.

The transformation to ordered ice X through the sequence ice VII → disordered ice X → ordered ice X, as suggested above, is also supported by the comparison with O-H…O systems at ambient. For O-O distances, $d_{\text{O-O}}$, varying from 3 to 2.44 Å, the O-H…O bond in those systems evolves from a proton double-well potential with a localized proton to a proton ordered symmetric bond. The intermediate state between these two configurations corresponds, for O-O distance around 2.52 Å, to a proton disordered system with a double minimum.[35] The isotopic ratio, which is around 1.35 for large $d_{\text{O-O}}$, exhibits a minimum for $d_{\text{O-O}} \sim 2.52$ Å and then increases to 1.4 for $d_{\text{O-O}} \sim 2.44$ Å. A comparison with the expected isotopic ratio of ice vs $d_{\text{O-O}}$ suggests that the single-well potential may be reached for $d_{\text{O-O}} \sim 2.32$ Å; that is, for pressure around 90 GPa. This is very likely a lower boundary for the pressure of transformation to the ordered symmetric ice.[12]

CONCLUSION

The equation of state of ice VII (H_2O) has been determined up to 106 GPa. Deviatoric strain corrections indicated that the experimental pressure is overestimated by about 3% in the whole pressure range, while the correction on the lattice parameter, depending on the *hkl* index, may reach 1%. The analysis of our data with the Vinet *et al.* EOS allowed us to disclose three pressure domains; higher-order phase transformations occur very likely around 12 and 66 GPa. According to recent investigations, we have checked that on deuteration these transitions shift to 18 and 82 GPa, respectively, which correspond to the pressure ranges where the proton disorder is expected to modify, as found from the analysis of the pressure dependence of the VII-VIII transition temperature. The present results in the region above 60 GPa appear to be consistent with the infrared investigations in the megabar range.

APPENDIX

The Birch-Murnaghan and Vinet equations of state are respectively given by

$$p=\frac{3}{2}B_0x^{-5}(1-x^{-2})\left[\frac{3}{4}(B_0'-4)(1-x^{-2})-1\right], \quad \text{(A1)}$$

$$p=\frac{3B_0(1-x)}{x^2}\exp\left[\frac{3}{2}(B_0'-1)(1-x)\right], \quad \text{(A2)}$$

with

$$x=\frac{a}{a_0},$$

and where B_0 and B_0' are the bulk modulus at zero pressure and its pressure derivative.

[1] J. P. Poirier, Nature (London) **299**, 683 (1982).
[2] W. Kuhs, J. L. Finney, C. Vettier, and D. V. Bliss, J. Chem. Phys. **81**, 3612 (1984).
[3] P. Pruzan, J. C. Chervin, and M. Gauthier, Europhys. Lett. **13**, 81 (1990).
[4] P. Pruzan, J. C. Chervin, and B. Canny, J. Chem. Phys. **99**, 9842 (1993).
[5] J. Eckert, C. R. Fincher, J. A. Goldstone, and W. Press, J. Chem. Phys. **75**, 3012 (1981).
[6] G. Samara and P. S. Peercy, Solid State Phys. **36**, 1 (1981).
[7] G. Samara and D. Semmingsen, J. Chem. Phys. **71**, 1401 (1979).
[8] P. Pruzan, J. Mol. Struct. **322**, 279 (1994).
[9] K. S. Schweizer and F. H. Stillinger, J. Chem. Phys. **80**, 1230 (1984).
[10] B. Silvi, J. Mol. Struct. **325**, 77 (1994).
[11] J. M. Besson *et al.*, Phys. Rev. B **49**, 12 540 (1994).
[12] P. Pruzan *et al.* (unpublished).
[13] K. Aoki, H. Yamawaki, M. Sakashita, and H. Fujihisa, Phys. Rev. B **54**, 15 673 (1996).
[14] A. F. Goncharov *et al.*, Science **273**, 218 (1996).
[15] L. Liu, Earth Planet. Sci. Lett. **61**, 359 (1982).
[16] R. G. Munro, S. Block, F. A. Mauer, and G. Piermarini, J. Appl. Phys. **53**, 6174 (1982).
[17] R. J. Hemley *et al.*, Nature (London) **330**, 737 (1987).
[18] J. Hama and K. Suito, Phys. Lett. A **187**, 346 (1994).
[19] H. Schlosser and J. Ferrante, J. Phys. Chem. Solids **52**, 635 (1991).
[20] J. C. Chervin, B. Canny, J. Besson, and P. Pruzan, Rev. Sci. Instrum. **66**, 2595 (1995).
[21] H. K. Mao, P. M. Bell, J. W. Shaner, and D. Steinberg, J. Appl. Phys. **49**, 3276 (1978).
[22] R. O. Piltz *et al.*, Rev. Sci. Instrum. **63**, 700 (1992).
[23] A. Hammersley (private communication).
[24] J. Rodriguez-Carvajal (private communication).
[25] A. K. Singh and G. C. Kennedy, J. Appl. Phys. **45**, 4686 (1974).
[26] N. Funamori, T. Yagi, and T. Uchida, J. Appl. Phys. **75**, 4327 (1994).
[27] A. K. Singh and C. Balasingh, J. Appl. Phys. **48**, 5338 (1977).
[28] H. Shimizu, M. Ohnishi, S. Sasaki, and Y. Ishibashi, Phys. Rev. Lett. **74**, 2820 (1995).
[29] H. Shimizu, T. Nabetani, T. Nishiba, and S. Sasaki, Phys. Rev. B **53**, 6107 (1996).
[30] R. E. Gagnon, H. Kiefte, M. J. Clouter, and E. Whalley, J. Chem. Phys. **92**, 1909 (1990).
[31] C. A. Tulk, R. E. Gagnon, H. Kiefte, and M. J. Clouter, J. Chem. Phys. **104**, 7854 (1996).
[32] P. Vinet, J. Ferrante, J. R. Smith, and J. H. Rose, J. Phys. C **19**, L467 (1986).
[33] J. P. Poirier, *Introduction to the Physics of the Earth's Interior* (Cambridge University Press, Cambridge, 1991), p. 66.
[34] K. R. Hirsch and W. B. Holzapfel, J. Chem. Phys. **84**, 2771 (1986).
[35] A. Novak, Struct. Bonding (Berlin) **18**, 177 (1974).